# Association Behavior of Poly (methyl methacrylate-b-methacrylic acid-b-methyl methacrylate) in Aqueous Medium

Jia Yao[1], Palaniswamy Ravi[1], Kam C. Tam[1], and Leong H. Gan[2]

[1]Singapore-MIT Alliance, School of Mechanical and Production Engineering, [2]Natural Science,

National Institute of Education, Nanyang Technological University, 50 Nanyang Avenue,

SINGAPORE 639798

*Abstract*—ABA type tri-block amphiphilic polyelectrolyte consisting of poly(methyl methacrylate-block-methacrylic acid-block-methyl methacrylate) (P(MMA-b-MAA-b-MMA)) was synthesized by atom transfer radical polymerization technique (ATRP) and the self-assembly behavior of the polymers in aqueous solution was studied over the course of neutralization. Combination of potentiometric and conductometric titrations along with dynamic light scattering (DLS) techniques were used to investigate the size and shape of aggregates at various degrees of neutralization. The effect of hydrophobic-hydrophilic (MMA-MAA) ratio and polymer chain length on the aggregation behavior during neutralization was studied. P(MMA-b-MAA-b-MMA) with longer MMA segment self-assembles via the close association mechanism through stronger self-entanglement of MMA chains, whereas P(MMA-b-MAA-b-MMA) with shorter MMA chain self-assembles via the open association mechanism, as confirmed by transmission electron microscopy (TEM). Conductometric titration was used to determine the counterion condensation during the course of neutralization. When the charge density of micelle approaches a critical value as neutralization progresses, counterion condensation of Na+ ions on the polymer chains occurs. The effect of counterion condensation on the aggregation behavior during neutralization was elucidated.

*Index Terms*—laser light scattering, MMA-b-MAA-b-MMA, potentiometric titration, self-assemble

## I. INTRODUCTION

Self-assembly of block copolymers in selective solvents can produce structures such as micelles, vesicles and physical networks, which have potential applications ranging from controlled release to rheological modifications.[1] With the advances made in the synthesis of block copolymers, specific macromolecular architecture can be tailored for specific applications.[2] By varying the block lengths or adjusting the pH and ionic strength of the solution, one can control the size, shape and the aggregation number of micelles.[3] An understanding on the structure-property relationship of block copolymeric micelles is important for the development of such systems for specific end use applications. Recently, much interest is focused on the theoretical models describing the structure of charged polyelectrolyte micelles.[4] Theories for both micelles and polymer brushes have been developed for "quenched polyelectrolyte", where the charges are fixed along the polymer chain, and for "annealed" systems, where the charge distribution is allowed to vary along the polymer chain, as in weak polyacids or polybases[5]. In annealed polyelectrolyte micelles and brushes, the pH controls the degree of charge on the micelle corona or polymer brush and can induce swelling due to electrostatic repulsions[6].

Systematic studies on polyelectrolyte amphiphilic block copolymers of poly(styrene-*block*-methacrylic acid) (PS-*b*-MAA)[7] and poly(styrene-*block*-acrylic acid) (PS-*b*-PAA)[8] with respect to micellar size and structure have been reported. Hybrid polymeric micelles with compact polystyrene core and poly(methacrylic acid)/poly(ethylene oxide) shells were produced in 1,4-dioxane(80 vol%)/ water mixture.[9] Because of the hydrophobic character of polystyrene, sample solutions were prepared either by heating for significantly long time or by stepwise dialysis from organic solvent to water, which limits the potential application of these systems. By selecting a less

hydrophobic segment such as poly(methyl methacrylate) (PMMA) with relatively high $T_g$, the solubility can be increased. In addition, the α-methyl groups on the MAA chain behave quite differently from PAA system where the conformation of the MAA at low pH is much more compact than the PAA.[10]

We reported previously a detailed study on the micellization behavior (size and shape) of P(MMA-*b*-MAA) polymer with different MMA/MAA ratio and segment lengths.[11] However, the aggregation behavior of tri-block ABA type polyelectrolyte system is much more complex and such system exhibits interesting micellization property in aqueous solution during the course of neutralization. Very recently, the aggregation behavior ABA type polyelectrolyte polymer of poly(acrylic acid)-*block*-poly(2-vinyl pyridine)-*block*-poly(acrylic acid) was reported.[12] Depending on the pH, the morphology of the polymer changes from single chain to network like structure to simple core shell micelles. Studies on such system are scare, and this provides the right motivation for the present study.

The objective of this paper is to investigate the micellization behavior of ABA type tri-block P(MMA-*b*-MAA-*b*-MMA) polymer during neutralization in aqueous solution, as information on the microstructural evolution is currently not available. Tri-block P(MMA-*b*-MAA-*b*-MMA) polymer dissolved in aqueous solution can form micelle that differs from di-block system due to the hydrophobic segments on both ends of PMAA chain. The micellar structure of di-block copolymer consists of hydrophobic MMA core and hydrophilic MAA corona and this morphology may be regarded as a convex polyelectrolyte brush. However, tri-block polymer may form open or close aggregation depending on the hydrophobic segment length. Scheme 1 illustrates the two possible aggregation mechanisms of tri-block polymers in aqueous environment where the mechanism is controlled by the balance between the hydrophobic and hydrophilic segments.
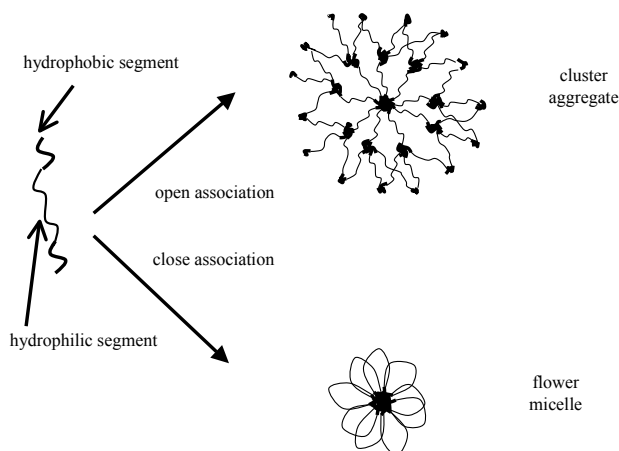


Scheme 1. The possible aggregation mechanisms for tri-block copolymers in aqueous environment.

**Materials**

*tert*-Butyl methacrylate (tBMA, Aldrich, 98%) was passed through a basic alumina column, stirred over CaH₂ and distilled under reduced pressure. Methyl methacrylate (MMA, Aldrich, 98%) was stirred over CaH₂ and distilled under vacuum. CuCl (99.98%,), N,N,N',N',N'',N''-hexamethyltriethylenetetramine (HMTETA), diethyl *meso*2,5-dibromo adipate (DEDBA), anisole were purchased from Aldrich and used without further purification.

**Synthesis of difunctional poly(tert-butyl methacrylate) (P(tBMA)) macroinitiator**

All synthetic steps were carried out under an argon atmosphere. In a typical experiment, CuCl, DEDBA and magnetic bar were introduced into a pre-dried Schlenk flask and tightly sealed with rubber septum. Deoxygenated anisole (50% vol with respect to monomer), and subsequently the monomer were introduced into the flask via an Ar-washed syringe and stirred until the system became homogeneous. Three "free-pump-thaw" cycles were performed to remove oxygen from the polymerization solution. Finally, degassed ligand (HMTETA) was introduced using Ar purged syringe and the flask was placed in a thermostated oil bath at 90°C. As soon as the ligand was added, the system turned dark green indicating the progress of the polymerization. After 80 min, the polymer was isolated by dissolving in tetrahydrofuran (THF) and passing through alumina column to remove the catalyst. Finally, the polymer was recovered by precipitating into 10 folds excess of water/methanol (1:1) mixture, filtered and dried under vacuum to constant weight. Yield =84%.

**Purification of Macroinitiator**

The macroinitiator was dissolved in acetone and stirred with DOWEX MSC macroporous ion-exchange resin for about 1 hr and the solution was filtered by passing through an alumina column. The solvent was partially removed by rotary evaporation and the polymer was precipitated by adding into 10 folds excess of water/methanol (50:50) mixture. The solid was filtered and dried under vacuum.

**Synthesis of P(MMA-*b*-tBMA-*b*-MMA) copolymer**

A known amount of di-functional P(tBMA) macroinitiator and CuCl were introduced into a Schlenk flask and tightly sealed with rubber septum. Degassed MMA monomer and 50 vol% (with respect to monomer) of anisole were introduced through Ar-purged syringe. The reaction mixture was degassed three times using freeze-pump-thaw cycle. Finally, degassed ligand (HMTETA) was introduced using an Ar-purged syringe and the flask was placed in an oil bath, which was thermostated at 60°C. After the reaction was completed, the catalyst was removed by passing through an alumina column and the polymer was recovered by precipitation in cold methanol. Subsequently the *tert*-butyl groups of the P(tBMA) blocks were hydrolyzed with concentrated hydrochloric acid in

dioxane at 85 °C for 6 hrs to form PMAA blocks and the block copolymer was precipitated in n-hexane. The polymer was washed with n-hexane for several times and dried under vacuum. FT-IR (KBr-pellet) showed the broad peak at 3500cm⁻¹, which is the characteristic absorption for carboxylic acid, and the content of the acid was quantified by potentiometric titration.

## Polymer Characterization

*Gel Permeation Chromatography:* Polymer molecular weights and molecular weight distributions were determined using gel permeation chromatography (GPC). Agilent 1100 series GPC system equipped with a LC pump, PLgel 5µm MIXED-C column and RI detector was used and the flow rate was maintained at 1.0 mL min⁻¹. The column was calibrated with narrow molecular weight polystyrene standards. HPLC grade THF stabilized with BHT was used as a mobile phase.

*Nuclear Magnetic Resonance Spectroscopy (NMR):* $^1$H NMR spectrum for the precursor block copolymer was measured using a Brüker DRX400 instrument in CDCl₃. The $^1$H NMR spectrum of the block copolymer allows the molar composition to be determined from the relative intensity at 1.42 ppm (-C(CH₃)₃ of the tBMA block) and 3.69 ppm (-OCH₃ of MMA block).

Table 1 Molecular Characteristics of ABA polyelectrolyte precursor

| Sample | $M_n^a$ | $M_w/M_n$ | Composition$^b$ (mol%) | | Degree of polymerization | |
|---|---|---|---|---|---|---|
| | | | tBMA | MMA | tBMA | MMA |
| Polymer A | 17200 | 1.21 | 85 | 15 | 114 | 20 |
| Polymer B | 18900 | 1.23 | 53 | 47 | 82 | 74 |
| Polymer C | 32600 | 1.20 | 26 | 74 | 76 | 218 |

$^a$ Calculated by GPC
$^b$ Composition calculated by 1H NMR spectroscopy
$^c$ Degree of polymerization calculated from the combination of GPC & 1H NMR data

## Preparation of P(MMA-*b*-MAA-*b*-MMA) Polymer Solution

In order to remove traces of impurity, the tri-block copolymers were dissolved in methanol and dialyzed against water for several days. The P(MMA-*b*-MAA-*b*-MMA) polymer was not directly soluble in aqueous medium at neutral pH. The polymer test solutions were prepared by titrating the polymer solution with 1M NaOH solution to a pH of ~11 and were continuously stirred until they became homogeneous, and then the pH was readjusted to ~3 using 1M HCl solution. The polymer solution remained transparent, confirming the homogeneity of the solution, which was subsequently used for the potentiometric and conductometric studies.

## Potentiometric and Conductometric Titrations

The pH and conductometric titrations were performed using an ABU93 Triburette Titration system equipped with a Radiometer pHG201 pH glass, Radiometer REF201 reference and conductivity electrodes. All the titrations were performed at 25°C, in a titration vessel filled with 100ml of 0.01~0.04wt% P(MMA-*b*-MAA-*b*-MMA) block copolymer solution subjected to constant stirring. A 1M standard NaOH solution (from Merck) was used as titrant. One minute of lag time was allowed between each dosage, in order to ensure that the acid-base reaction has reached equilibrium.

## Laser Light Scattering (LLS)

The laser light scattering experiments were conducted using a Brookhaven laser light scattering system. This system consists of a BI200SM goniometer, BI-9000AT digital correlator and other supporting data acquisition and analysis software and accessories. An argon-ion vertically polarized 488nm laser was used as the light source. The $G_2(t)$ function obtained from dynamic light scattering (DLS) were analyzed using the Inverse Laplace Transformation technique (Regularized Positive Exponential Sum (REPES)[13] in our case) to produce the distribution function of decay time. The concentration of the polymer solutions investigated by light scattering is 0.01~0.04wt%, which is in the dilute solution regime where the behavior of individual particles can be characterized. The hydrodynamic radii ($R_h$) of micelles were obtained by Stokes-Einstein equation: $R_h = \dfrac{kT}{6\pi\eta D}$, where $kT$ is the thermal energy factor, $\eta$ is the temperature-dependent viscosity of solvent and D is the diffusion coefficient calculated from DLS data. Several measurements were carried out at 90$^o$ for a given sample to obtain an average hydrodynamic radius and the variation in the $R_h$ values is small.[14] Measurements of dynamic light scattering and static light scattering were performed at different scattering angles and sample concentrations. From static light scattering (SLS), the molecular weights ($M_w$) and gyration radii ($R_g$) of micelles were measured using Zimm, Berry or Debye plots.[8]

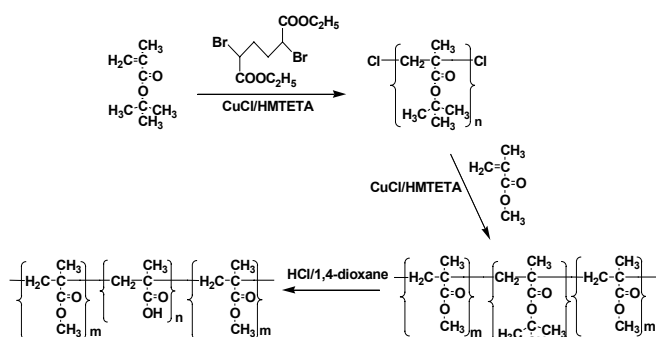## Transmission Electron Microscopy (TEM)

Observations by TEM (JEOL 2010, 200KV) were performed on the polymeric systems. One or two drops of a selected solution were placed onto a carbon coated copper grid, and the sample on the copper grid was then dried in a desiccator for 24 hours before characterized under TEM instrument.

### III. RESULTS AND DISCUSSION

## Synthesis of Tri-block P(MMA-*b*-tBMA-*b*-MMA) Polymer

Though the polymerization of tBMA and its di-block copolymers by ATRP technique was reported recently by our group[11], controlled polymerization of tri-block ABA type copolymerization with MMA has not been reported so far. The di-functional P(tBMA) macroinitiator was

synthesized using a difunctional initiator of diethyl *meso* 2,5-dibromo adipate (DEDBA) and CuCl/HMTETA catalyst system in anisole at 90°C. Polymerization was stopped when it became slightly viscous(<90% conversion) to maintain the high end functionality. It was proven that by using CuCl as a cross catalyst, more stable –Cl end groups were formed. Molecular weight distribution of the homopolymers determined by GPC was slightly higher ($M_w/M_n$ of 1.28) and this may be due to the slight structural dissimilarity of the initiator with respect to the monomer. Tri-block copolymer was synthesised using the di-functional macroinitiator with the same catalyst system (CuCl/HMTETA) in anisole at 60°C. The polymer was precipitated from methanol and the polydispersity of the purified polymers was lower (1.20-1.23), which is probably due to the solubility of the oligomers in methanol as the P(tBMA) is soluble in methanol. Scheme 2 shows the synthesis route.



Fig 1. GPC chromatographs for homopolymer and ABA tri-block copolymers of P(MMA-b-tBMA-b-MMA). A Homopolymer PtBMA$_{81}$; B P(MMA$_{37}$-b-tBMA$_{82}$-b-MMA$_{37}$); C P(MMA$_{109}$-b-tBMA$_{76}$-b-MMA$_{109}$)



Scheme 2. Synthesis of ABA tri-block copolymer



Fig. 2. Molar composition of ABA tri-block copolymer was determined from the ^{1}H NMR spectrum using the relative intensity at 1.42 ppm (-C(CH$_3$)$_3$ of the tBMA block) and 3.69 ppm (-OCH$_3$ of MMA block). P(MMA$_{37}$-b-tBMA$_{82}$-b-MMA$_{37}$) as example.

Fig 1 shows the GPC chromatograms for homopolymer and ABA tri-block copolymers of P(MMA-b-tBMA-b-MMA). From the fig, it can be observed that the controlled polymerisation of ABA tri-block copolymers was obtained with narrow polydispersity. As the molecular weights are in good correlation with the theoretical molecular weights with low polydispersity, we did not focus on the detailed studies on the kinetics of the polymerisation process. The molar composition of the ABA tri-block copolymer was determined from the ^{1}H NMR spectrum (Fig 2) using the relative intensity at 1.42 ppm (-C(CH$_3$)$_3$ of the tBMA block) and 3.69 ppm (-OCH$_3$ of MMA block).

The detail molecular weights and polydispersities of the polymers are given in Table 1.

**Titration Studies**

From the titration, both the conductivity and pH curves were obtained simultaneously. These two curves reveal the changes in the concentrations of different ions. The s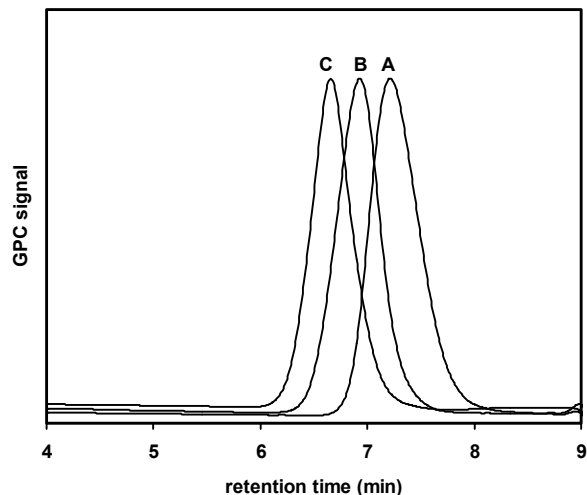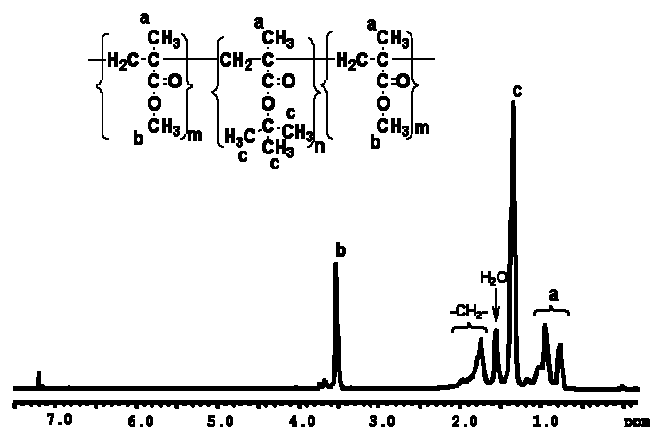ystems being investigated contain the following ions: H$^+$, Na$^+$, OH$^-$, Cl$^-$, and macroion, and the conductivity can be expressed as follows: [15]

$$\Lambda = C_{Na^+}\lambda_{Na^+} + C_{H^+}\lambda_{H^+} + C_{OH^-}\lambda_{OH^-} + C_{Cl^-}\lambda_{Cl^-} + C_P\lambda_P \quad (1)$$

where, $C_i$ is the concentration of free ion in solution, and $\lambda_i$ is the molar conductivity of the corresponding ion. During titration, the concentration of Cl$^-$ ion remains constant, while the larger macro-ions (denoted by "P") do not contribute much to the conductivity; hence the conductivity curve reflects the concentration changes of H$^+$, Na$^+$ and OH$^-$. Fig 3 shows the conductivity curve as a function of moles of 1M NaOH titrated to 0.011wt% of polymer B. The titration curve can be divided into three regimes, based on the changes in the slope of the conductivity curve. Region 1 represents the neutralization reaction between excess HCl and NaOH, where the decrease in conductivity is caused by the decrease in the concentration of H$^+$ ion, since the mobility of H$^+$ ($\lambda_{H^+}^0$ = 350 S·cm$^2$/mol, 25°C) is much larger than that of Na$^+$($\lambda_{H^+}^0$ = 50.5 S·cm$^2$/mol, 25°C)[14], even though the concentration of Na$^+$ has also
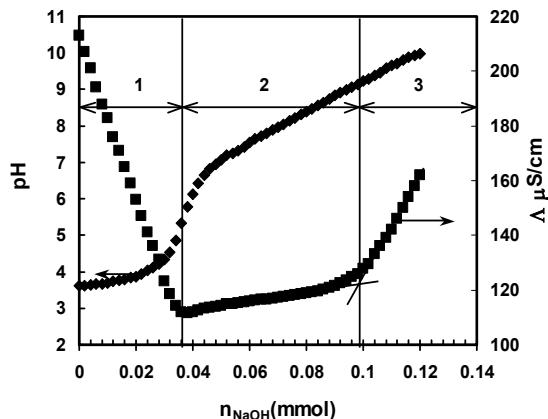
Fig 3. Titration curves of 0.011wt% P(MMA$_{37}$-b-MAA$_{82}$-b-MMA$_{37}$), ◆ pH, ■ conductivity, the conductivity curve shows more obvious change than pH curve during the neutralization process.

increased. Region 2 corresponds to the reaction between MAA segments and NaOH where the increase in the conductivity is mostly attributed to the increase in the concentration of Na$^+$ ion. In this region, the concentration changes of H$^+$ and OH$^-$ can be calculated from the pH values, and they are very small and can be neglected compared to Na$^+$ ion. Thus, the conductivity curve in region 2 reflects the change in free Na$^+$ ion concentration. Region 3 represents the excess NaOH, where the Na$^+$ and OH$^-$ contribute to the large increase in the conductivity.

From the pH curve, we observed a sharp change at ~ 0.035 mmol of NaOH, at the transition between region 1 and 2. The end point for complete neutralization of MAA can be deduced from the conductivity curve where a large increase in the conductivity is observed after all the carboxylic acid groups are neutralized. The concentration of polymer can also be determined from the titration based on the structure formula determined from NMR and GPC data.

### Potentiometric Titration

The conformational behavior of PMAA have been reported previously, where the polymer chains undergo strong hypercoiling with decreasing pH in the region of pH 6 to 5[10]. The base titration of polyelectrolyte aggregates permits a fundamental characterization of the microstructure.

The acid dissociation equilibria of weak acidic polyelectrolyte may be expressed by the equilibrium equation shown below:

$$HA \xrightleftharpoons{\;\;K_a\;\;} H^+ + A^-$$
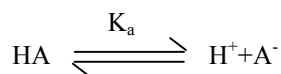
where HA is the acid and H$^+$ and A$^-$ are the hydrogen ion and corresponding anion. The equilibria can be quantified by defining the apparent acid dissociation constant, K$_a$,

which can be determined from the measured pH and the degree of dissociation α, at the equilibrium:

$$pK_a = pH + \log\left(\frac{1-\alpha}{\alpha}\right) \quad (2)$$

The pK$_a$ value reflects the overall acid dissociation equilibrium and is affected by the charge density on the polymer chains, and α can be estimated by the pH value and the amount of polyelectrolyte and the base added. For normal acids, such as CH$_3$COOH, the pK$_a$ is generally a constant. But for polyacids, such as poly acrylic acid (PAA), the pK$_a$ is not a constant, because the overall acidity depends on the degree of neutralization. The COO$^-$ groups on the polymer chain can hinder the dissociation of COOH groups, because it is more difficult to extract H$^+$ ions from the polymer to the solution due to the constraints of electrostatic attraction from COO$^-$ groups. Thus, the pK$_a$ curve provides useful information on the polymer structure, such as the charge density on the polymer chain.

Fig 4 shows the pK$_a$ curve plotted against degree of neutralization α obtained by titrating 1M NaOH into aqueous polymer solutions. The di-block copolymer P(MMA$_6$-b-MAA$_{54}$) was chosen for comparison. Depending on the block composition, different pK$_a$ curves were obtained.
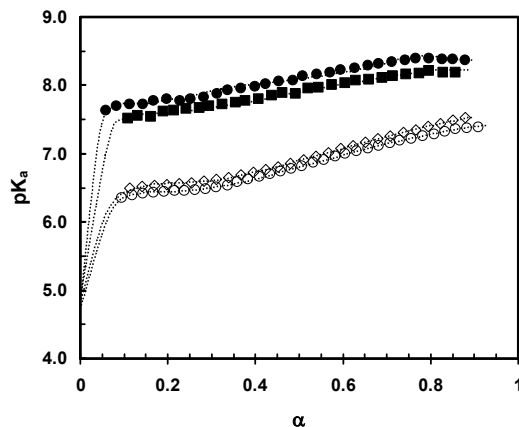


Fig 4. pK$_a$ curves of different polymer as a function of degree of ionization α. (1) ◇ Polymer A, P(MMA$_{10}$-MAA$_{114}$-MMA$_{10}$) (2) ● Polymer B, P(MMA$_{37}$-b-MAA$_{82}$-b-MMA$_{37}$) (3) ■ Polymer C, P(MMA$_{109}$-MAA$_{76}$-MMA$_{109}$) (4) Di-block copolymer, ○ P(MMA$_6$-MAA$_{54}$) There are similar trends between P(MMA$_{10}$-MAA$_{114}$-MMA$_{10}$) and P(MMA$_6$-MAA$_{54}$), and both of the curves show a flat part at 0.15<α<0.3. The curves of P(MMA$_{37}$-MAA$_{82}$-MMA$_{37}$) and P(MMA$_{109}$-MAA$_{76}$-MMA$_{109}$) show an increase, but with a lower slope.

For di-block copolymer with chemical composition P(MMA$_6$-b-MAA$_{54}$), a clear transition occurs at α ~ 0.3. The slope appears to be small at α<0.3, and becomes larger at α>0.3. During neutralization, the acidity of the polymer decreases due to the increasing charge density, which hinders further dissociation of COOH groups, and this is reflected by the increase in pK$_a$. The α-methyl groups on the MAA chain are partly hydrophobic, and the hydrophobic interactions between α-methyl groups induce coiling of MAA chains at low degree of neutralization. At

the neutral state ($\alpha=0$), where the electrostatic potential is completely diminished, the pK$_a$ is ~ 4.8 for all MMA with different chain lengths or at different salt concentrations [16]. The sharp increase in the pK$_a$ at $\alpha<0.15$ corresponds to compact structure of the aggregates where the charge density increases rapidly when NaOH was added. At the critical point of $\alpha\sim0.15$ the compact aggregates begin to uncoil when the electrostatic repulsion can compensate hydrophobic forces, which induces swelling of the aggregates without destroying the hypercoil chain structure. In the hypercoil chain structure, COOH and COO$^-$ groups are located on the exterior with $\alpha$-methyl groups situated within the interior of the hypercoil, and this enhances the surface charge density of the aggregate. Further neutralization enhances the polymer charge density, where the electrostatic repulsion force exceeds that of the hydrophobic interaction. The spacing between COO$^-$ groups on the polymer backbone is enhanced by electrostatic repulsion, which destroys the ordered structure as evident by the flat region of pK$_a$ curve at $0.15<\alpha<0.3$. When we compared this transition with the R$_h$ data from light scattering experiments, we observed that the particle size increases from ~23 nm to ~32 nm between $\alpha$ of 0 and 0.3, and it then remains constant at around 33nm for larger $\alpha$. This behavior is probably caused by the counter-balancing effect of counterion condensation, which suppresses the electrostatic repulsive forces.[11]

The pK$_a$ curve of polymer A exhibits similar behavior as di-block copolymer, P(MMA$_6$-b-MAA$_{54}$), where the slope is rather flat for the region $0.15<\alpha<0.3$, suggesting that the polymer exhibits a transition from compact coil to stretched chain. The short MMA chains at both ends are unable to significantly restrict the polymer stretching induced by the neutralization of MAA segments. Hence the polymer chains most likely associate via the open association mechanism. The pK$_a$ of longer hydrophobic segments (polymer C) shows a smooth increase with the degree of neutralization, suggesting that there is no obvious transition from compact coil to stretched chain. The long segments of MMA, due to its high T$_g$ could have restricted the dynamics of MAA stretching. The pK$_a$ curve of polymer B also exhibits similar trend as polymer C, indicating that the hydrophobicity of the polymer attributed to longer MMA segment (37 MMA units in polymer B) is sufficient to produce aggregate via the close association mechanism, since their pK$_a$ curves are fairly similar.

**Conductometric Titration[17]**

Fig 5 shows the conductometric titration curves of the tri-block polymers. The conductivity curve of polymer A shows a clear inflection at 0.054 mmol of NaOH (which corresponds to $\alpha\sim0.4$). The slope at low $\alpha$ region is larger than at high $\alpha$ (corresponding the range of region 2 in Fig 2). Based on Eq. (1), the conductivity in this region can be reduced to Eq. (3) since the major contribution to the conductivity is caused by the change in Na$^+$ concentration.

$$\Lambda = C_{Na^+}\lambda_{Na^+} + constant \quad (3)$$

where the $C_{Na^+}$ is the concentration of free Na$^+$ in solution. From Eq. (3), the linear increase in the conductivity is proportional to increase in mobile sodium ions, where the slope should correspond to $\lambda_{Na^+}$. In the conductivity curve of polymer A, before the inflection, it possesses a slope of 50 S·cm$^2$/mol (c.f. $\lambda_{Na^+}^0$ = 50.5 S·cm$^2$/mol, 25°C), after the inflection, the slope becomes 31.5 S·cm$^2$/mol. The slope change indicates the counterion condensation at high degree of neutralization. At low $\alpha$, most of the Na$^+$ ions added are mobile or free, however at higher $\alpha$, the negative charge density on the micelles is sufficiently strong to attract the oppositely charged ions, resulting in the counterion condensation of Na$^+$ on the negatively charged sites. Thus, beyond a certain value where counterion condensation occurs, added Na$^+$ ions condense on the micelles, resulting in an overall reduction in free Na$^+$ ions. This phenomenon can be identified by the inflection at $\alpha$ ~ 0.4, which is the onset point for counterion condensation process.

Base on Eq.3, the free Na$^+$ ions concentration can be tracked by conductivity measurement. $C_{Na^+}$ can be expressed as $C_{Na^+} = (1 - r_{cond}) \cdot C_{Na^+}^0$, where $r_{cond}$ is the proportion of sodium ions added that are condensed after the onset point, $C_{Na^+}^0$ is the amount of sodium ions added. $\lambda_{Na^+}$ is a constant as environment does not change much, and the proportion of condensed sodium ions can also be treated as a constant. $k_{high}$ is the slope of conductivity curve after the onset point for counterion condensation, which equals $(1 - r_{cond}) \cdot \lambda_{Na^+}$, and $k_{low}$ is the slope of conductivity curve before the onset point for counterion condensation, which equals $\lambda_{Na^+}$. From the ratio of the two slopes, the proportion of condensed sodium ions can be determined using the following expression:

$$r_{cond} = 1 - k_{high} / k_{low} \quad (4)$$

The $r_{cond}$ value of 0.37 was obtained for polymer A using Equation (4).

The conductivity curves for polymer B and polymer C differ from the curve of polymer A. They do not show obvious inflections at the corresponding region, and the slopes are much lower than that of polymer A. This phenomenon may explain the effect of hydrophobicity on the aggregation behavior of the polymer. Because of strong hydrophobic interaction, polymer C tends to form compact close association with ~200-300 polymer chains (Fig 6, the aggregation number was calculated by $N_{agg} = \dfrac{M_{w,micelle}}{M_{w,unimer}}$, the measurement of $M_{w,micelle}$ is described in laser light scattering part.), and the mobility of MAA segments is severely hindered. During the

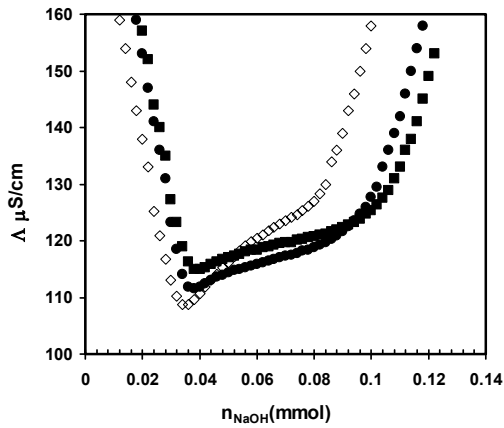Fig 5. Conductivity curves of different polymers correspond to the amount of NaOH added: (1) ◇ A P(MMA$_{10}$-MAA$_{114}$-MMA$_{10}$) (2) ● B P(MMA$_{37}$-b-MAA$_{82}$-b-MMA$_{37}$) (3) ■ C P(MMA$_{109}$-MAA$_{76}$-MMA$_{109}$) The curve of P(MMA$_{10}$-MAA$_{114}$-MMA$_{10}$) shows an inflection at 0.054 mmol NaOH, which is the onset of counterion condensation where P(MMA$_{37}$-MAA$_{82}$-MMA$_{37}$) and P(MMA$_{109}$-MAA$_{76}$-MMA$_{109}$) curves do not show the inflection.

neutralization, the swelling of MAA segments induced by the electrostatic repulsion between COO⁻ groups is restricted by strong hydrophobic association of MMA blocks. Hence, the charge density on the aggregate is relatively high, which favors counterion condensation of Na⁺ ions on the aggregate at low degree of neutralization. The smaller slope in the conductivity curve indicates stronger Na⁺ condensation for polymer C. The slope of polymer B curve at this region is slightly larger than polymer C, which suggests that ionized MAA segments are able to swell to a certain degree. This lowering of the charge density reduces the amounts of condensed counterion.

From the conductivity curves, we can conclude that the less hydrophobic polymer A (short MMA segment) could not restrict the swelling of MAA segments during neutralization, hence the polymer chains aggregate via the open association process to produce larger aggregates containing 1000 to 4000 polymer chains (Fig 6). The strong hydrophobicity of polymer C hinders the swelling of MAA segments, which favors the close association
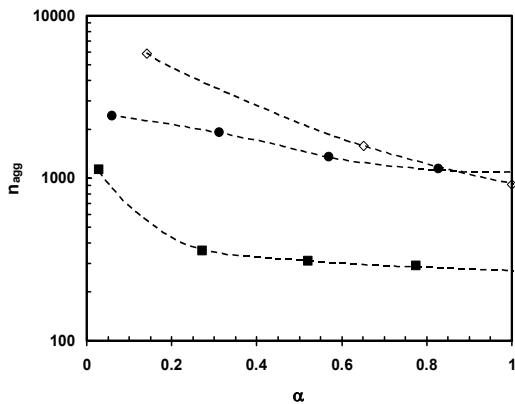


Fig 6. Aggregation numbers (N$_{agg}$) of three polymers as a function of degree of ionization: (1) ◇ A P(MMA$_{10}$-MAA$_{114}$-MMA$_{10}$) (2) ● B P(MMA$_{37}$-b-MAA$_{82}$-b-MMA$_{37}$) (3) ■ C P(MMA$_{109}$-MAA$_{76}$-MMA$_{109}$)

process. Polymer B exhibits similar property to polymer C, except the hydrophobic MMA segment is shorter, thus mixtures of aggregate produced from open and close association are believed to be present.

**Laser Light Scattering**

The laser light scattering experiments provide additional insights on the morphology of the aggregate during the neutralization process. Fig 7 shows the R$_h$ distribution function of the polymer A and polymer C at different neutralization degrees.

The R$_h$ distribution function of polymer A shows a major peak of large particles (~85 nm). At high degree of



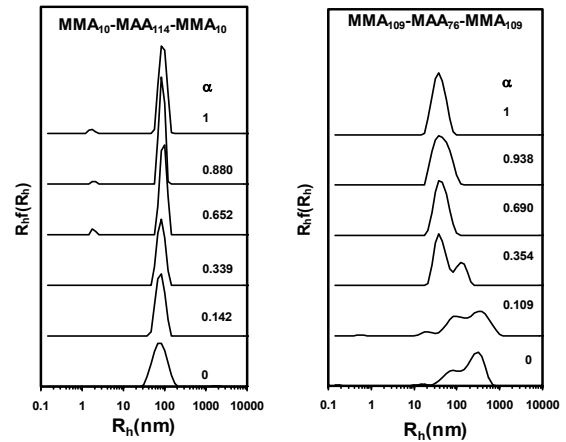Fig 7. Evolution of R$_h$ distribution functions during the ionization of P(MMA$_{10}$-MAA$_{114}$-MMA$_{10}$) and P(MMA$_{109}$-MAA$_{76}$-MMA$_{109}$). The DLS were measured at 90°.

neutralization, one small peak representing smaller particles (~2 nm) can be observed, and this peak may be related to unimers. At low degree of neutralization, α<0.3, the major slow peak is broad, and further neutralization makes the peak narrower. The entanglements of MAA segments at low α leads to larger aggregates, which are destroyed by electrostatic repulsion and the large aggregates dissociate into smaller ones that are held together by hydrophobic MMA segments, which agrees with the trend in the pK$_a$ curve.

For polymer C, the distribution function exhibits an obvious size reduction at α<0.3 due to disentanglement of MAA segments. Further neutralization produces stronger electrostatic repulsion, but the strong hydrophobic association of MMA segments retains the morphology of the aggregate.

Fig 6 shows the aggregation number determined from LLS measurements. The molecular weight was normally determined from extrapolation using the Zimm plot given by Eq 5.

$$\frac{Kc}{R(\theta)} = \frac{1}{M_w} \cdot \left[ 1 + \frac{R_g^2 q^2}{3} \right] + 2A_2 c \qquad (5)$$

where $K$ is the optical constant ($2\pi^2(n\ dn/dc)^2/\lambda^4 N_{Av}$), $n$ is the refractive index of the solvent, $dn/dc$ is the specific

refractive index increment, $\lambda$ is the wavelength in vacuum, $N_{Av}$ is Avogadro's number, c is the concentration, $R(\theta)$ is the Rayleigh ratio at the angle of measurement, $M_w$ is the weight-average molecular weight, $R_g$ is the z-average radius of gyration, $q$ is the scattering wave vector $((4\pi n/\lambda)\sin(\theta/2))$, and $A_2$ is the second virial coefficient. For particles of very high molecular weight (e.g., $>10^6$g/mol), or charged particles, $Kc/R(\theta)$ exhibits significant curvature in the angular dependence. In these cases, special care must be taken when analyzing the data.[18] Berry plot can be used to solve the problem.

For polymer C, an obvious decrease of apparent aggregation number was observed at $0<\alpha<0.3$, followed with a small decrease in the aggregation number at $\alpha>0.3$. This is consistence with results from DLS.

Fig 8 shows the evolution of $R_h$ distribution functions during course of neutralization of Polymer B, which exhibits similar trend as Polymer C, except a more obvious slow mode is observed. Due to the shorter MMA segments, the hydrophobicity of the Polymer B is insufficient to bend all the PMAA chains, thus some aggregates are produced via the open association mechanism. In open association process, polymer chains form bridges linking hydrophobic MMA cores to form large aggregates, which are not completely destroyed by electrostatic repulsion at high degree of neutralization. Such morphology is consistent with the trend depicted by the larger aggregation number that does not change significantly with neutralization degree as shown in Fig 6. The stability of the aggregates was also monitored by conducting DLS at different time intervals, and we observed that no obvious change had occurred after 10 days.

In order to see the relative population of follower-like micelles and clusters as the function of the concentration, we conducted the DLS at different concentration for polymer B at high neutralization degree. There is no concentration dependence of the relative population, till rather low concentration that the DLS can not properly measure the particle size. This phenomenon possibly means the two types of aggregates cannot maintain the
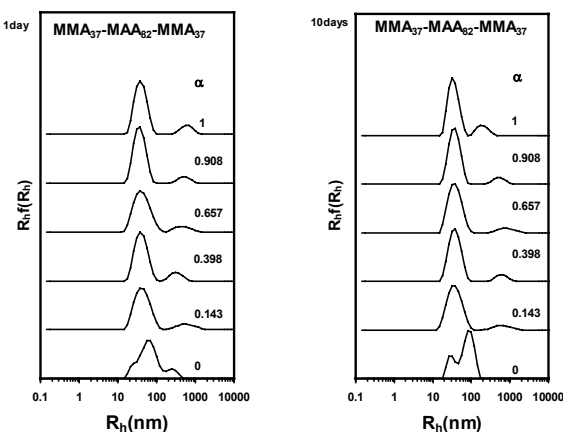
dynamic equilibrium in our case.

The apparent aggregation number of Polymer A is rather high, and it decreases during the course of neutralization. In this case the open association produces larger aggregates, and electrostatic repulsion is able to decrease the aggregation number.

The $R_h$ values of the three polymers at fully neutralized stages were calculated from relaxation time distribution functions. The hydrodynamic radii of the Polymer A, B, and C are 90, 36 and 40nm respectively. When the polymer is less hydrophobic (Polymer A), the chains aggregate via open association process to form multilayer particle (2-3 layers), and for more hydrophobic polymer (Polymer C) close association process produces flower-like or rosette micelle. At intermediate hydrophobic condition (Polymer B $P(MMA_{37}-MAA_{82}-MMA_{37})$), the flower-like micelle (36nm), co-exist with large aggregates (~500nm).

**Transmission Electron Microscopy (TEM)**

Fig 9 shows the TEM micrographs of the polymeric system obtained from aqueous solutions. The morphology of Polymer B $P(MMA_{37}-MAA_{82}-MMA_{37})$ from aqueous solution at pH=10 (Fig 9a), shows polymer cluster aggregates coexist with rosette micelles. The dark regions within the cluster aggregate correspond to the connection nodes consisting of hydrophobic MMA segments. The size of the cluster aggregates is around 400nm, if we consider the cluster shrinkage during sample drying, the value is quite consistent with the value from DLS. Fig 9b shows the TEM micrograph of Polymer C $P(MMA_{109}-MAA_{76}-MMA_{109})$ from aqueous solution at pH=10. It shows close association aggregates and the particles size is around 50nm in diameter, which is consistent with the results from DLS measurements as the shrinkage of MAA shell during sample drying was considered. From the aggregation number, the core size ($R_c$) can be estimated[19]. For polymer C at pH=10, the $R_c$ is about 13nm, where the $R_h$ is 40nm, so the shell has the thickness about 27nm (contributed from 76 MAA units). The di-block polymer $P(MMA_6-MAA_{54})$ has the $R_h$ about 33nm at high pH, the $R_c$ is about 2nm, hence the shell thickness is about 31nm (contributed from 54 MAA units). So when we compare the shell thickness of these two cases, we can easily see the bent effect in the micelle from polymer C. This is also the evidence of close association of polymer C. The corresponding $R_g$ value is 28nm, then $R_g/R_h$ is 0.7, the value shows the core-shell structure of the aggregate. No polymer cluster aggregate is evident.

## IV. CONCLUSIONS

Well-defined amphiphilic ABA type polyelectrolytes of P(MMA-*b*-MAA-*b*-MMA) polymers were synthesized using ATRP. The self-assembly of the ABA tri-block polyelectrolytes with different hydrophobic lengths in aqueous medium were conducted using potentiometric and conductometric titrations and laser light scattering techniques. The MAA chain forms compact coil at low degree of neutralization due to the $\alpha$-methyl groups on the



Fig 8. Evolution of $R_h$ distribution function during the ionization for $P(MMA_{37}-MAA_{82}-MMA_{37})$, which was measured at 1 day and 10 days after preparation. The DLS were measured at 90°.

polymer backbone. At low degree of neutralization, ($\alpha$<0.3) the motion of MAA segments is not hindered by MMA blocks, thus the polymer chains swell and uncoil. Counterion condensation occurs at $\alpha\sim0.4$ when the charge density is sufficiently high. For Polymer C with longer MMA chains, flower-like micelles with looping MAA chains are produced. Shorter MMA segments (polymer A) leads to open association, long MMA segments (polymer C) produces aggregate via the close association process, and moderate MMA segments (polymer B) leads to the coexistence of aggregates produced from closed and open association process.

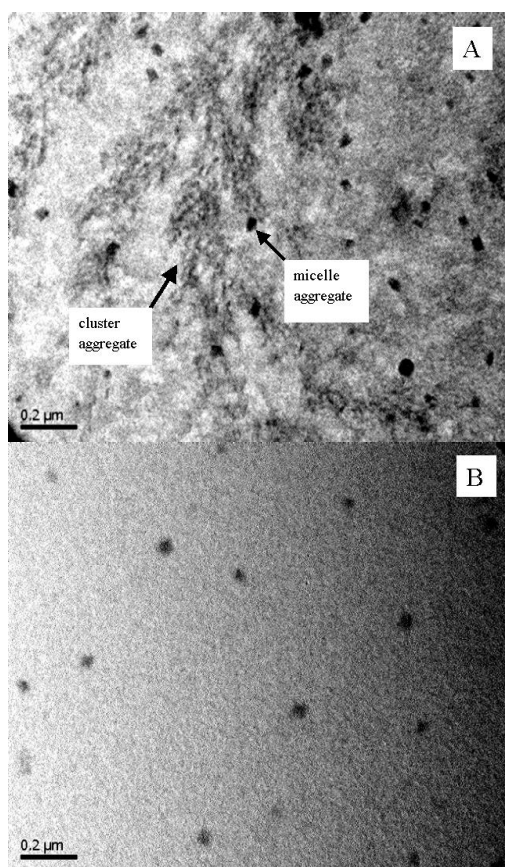Fig 9. (a) TEM micrograph of P(MMA$_{37}$-MAA$_{82}$-MMA$_{37}$) solution at pH=10 reveals the coexistence of cluster aggregate with close association particles; (b) TEM micrograph of P(MMA$_{109}$-MAA$_{76}$-MMA$_{109}$) solution at pH=10 confirming the presence of rosette micelles produced via the close association process.

REFERENCES

[1]   (a) Kwon, G. S.; Naito, M.; Yokoyama, M.; Okano, T., Sakurai, Y.; Kataoka, K. *Pham. Res*. **1995**, 12, 92. (b) Kataoka, K.; Kwon, G. S.; Yokoyama, M.; Okano, T.; Sakurai, Y. *J. Controlled Release* **1993**, 24,119. (c) Harada, A.; Kataoka, K. *Macromolecules* **1995**, 28, 5294. (d) Scholz, C.; Iijima, M.; Nagasaki, Y.; Kataoka, K. *Macromolecules* **1995**, 28, 7295.

[2]   (a) Sukhorukov, G.B.; Antipov, A.A.; Voigt, A.; Donath, E.; Mohwald, H. *Macromol. Rapid Commun*. **2001,** 22,44. (b) Sauer, M.; Meier, W. *Chem. Commun*. **2001,** 1, 55.

[3]   Zhang, X.; Matyjaszewski, K. *Macromolecules* **1999**, 32, 1763.

[4]   (a) Misra, S.; Varanasi, S.; Varanasi, P. P. *Macromolecules* **1989**, 22, 4173. (b) Pincus, P. *Macromolecules* **1991**, 24, 2912. (c) Dan, N.; Tirrell, M. *Macromolecules* **1993**, 26, 4310. (d) Shusharina, N. P.; Nyrkova, I. A.; Khokhlov, A. R. *Macromolecules* **1996**, 29, 3167. (e) Hariharan, R.; Biver, C.; Mays, J.; Russel, W. B. *Macromolecules* **1998**, 31, 7506.

[5]   (a) Zhulina, E. B.; Borisov, O. V. *Macromolecules* **1996**, 29, 2618. (b) Israels, R.; Leermakers, F. A. M.; Fleer, G. J. *Macromolecules* **1994**, 27, 3087.

[6]   (a) Baines, F. L.; Billinggham, N. C.; Armes, S. P. *Macromolecules* **1996**, 29, 3416. (b) Biesalski, M.; Rifihe, J.; Johannsmann, D. *J. Chem. Phys*. **1999**, 111, 7029. (c) Groenewegen, W.; Lapp, A., Egelhaaf, S. U.; van der Maarel, J. R. C. *Macromolecules* **2000**, 33, 4080.

[7]   (a) Prochazka, K.; Kiserow, D.; Ramireddy, C.; Tuzar, Z.; Munk, P.; Webber, S. E. *Macromolecules* **1992**, *25*, 454. (b) Ramireddy, C.; Tuzar, Z.; Prochazka, K.; Webber, S. E.; Munk, P. *Macromolecules* **1992**, *25*, 2541 (c) Prochazka, K.; Martin, T. J.; Munk, P.; Webber, S. E. *Macromolecules* **1996**, *29*, 6518. (d) Karymov, M. A.; Prochazka, K.; Mendenhall, J. M.; Martin, T. J.; Munk, P.; Webber, S. E. *Langmuir* **1996**, *12*, 4749. (e) Stepanec, M.; Podhajecka, K.; Prochazka, K.; Teng, Y.; Webber, S. E. *Langmuir* **1999**, *15*, 4185. (f) Stepanec, M.; Prochazka, K. *Langmuir* **1999**, *15*, 8800. (g) Kriz, T.; Masar, B.; Pospisil, H.; Plestil, J.; Tuzar, Z.; Kiselev, M.A. *Macromolecules* **1996,** 29, 7853.

[8]   (a) Zhang, L.; Eisenberg, A. *Science* **1995**, 268, 1728. (b) Zhang, L.; Eisenberg, A. *Macromolecules* **1996**, 29, 8805. (c) Zhang, L.; Shen, H.; Eisenberg, A. *Macromolecules* **1997**, 30, 1001. (d) Yu, K.; Zhang, L.; Eisenberg, A. *Langmuir* **1996**, 12, 5980.

[9]   Stepanec, M.; Podhajecka, K.; Tesarova, E.; Prochazka, K.; Tuzar, Z.; Brown, W. *Langmuir* **2001,** 17, 4240.

[10]   (a) Bednar, B.; Morawetz, H.; Shafer, J. A. *Macromolecules* **1985**, 18, 1940. (b) Koenig, J. L.; Angood, A. C.; Semen, J.; Lando, J. B. *J. Am. Chem. Soc.* **1969**, 91, 7250.

[11]   (a) Ravi, P.; Wang, C.; Tam, K.C.; Gan, L.H. *Macromolecules* **2003**, 36, 173-179. (b) Yao, J.; Ravi, P.; Tam, K.C.; Gan, L.H. *Langmuir, submitted*. (c) Gan, L.H., Ravi, P., Mao, B.W., Tam, K.C., *J. Polym. Sci., Polym. Chem., Part A, in press*.

[12]   Sfika, V.; Tsitsilianis, C. *Macromolecules* **2003**, 36, 4983.

[13]   Jakes, J. *Czech. J. Phys*. **1988**, B38, 1305.

[14]   (a) Dai, S; Tam, K. C.; Jenkins, R. D. *Macromolecules* **2001**, 34, 4673. (b) Dai, S; Tam, K. C.; Jenkins, R. D. *J. Phys. Chem. B* **2001**, 105, 10189.

[15]   Kolthoff, I. M.; Laitinen, H. A. *pH and electro titrations*; second edition, John Wiley & Sons, Inc. New York, USA, 1952.

[16]   Crescenzi, V.; Quadrifoglio, F.; Delben, F. *J. Polym. Sci. Pt A-2* **1972**, 10, 357.

[17]   Nagasawa, M.; Murase, T.; Kondo, K. *J. Phys. Chem*. **1965**, 69, 4005.

[18]   Kratochvil, P. *Classical Light Scattering from Polymer Solutions*; Jenkins, A. D., Ed.; Elsevier Science Publishers: New York, 1987.

[19]   Khougaz, K.; Astafieva, I.; Eisenberg, A. *Macromolecules* **1995**, 28, 7135.